ADVANCES IN ATMOSPHERIC SCIENCES, VOL. 39, APRIL 2022, 609–624

• **Original Paper** •

Seasonal Cumulative Effect of Ural Blocking Episodes on the Frequent Cold events in China during the Early Winter of 2020/21※

Yao YAO*[1,2], Wenqi ZHANG[1,2], Dehai LUO[1,2], Linhao ZHONG[1,2], and Lin PEI[3]

[1]*Key Laboratory of Regional Climate-Environment for Temperate East Asia*, *Institute of Atmospheric Physics*, *Chinese Academy of Sciences*, *Beijing* 100029, *China*

[2]*University of Chinese Academy of Sciences*, *Beijing* 100029, *China*

[3]*Institute of Urban Meteorology*, *China Meteorological Administration*, *Beijing* 100029, *China*

(Received 16 March 2021; revised 17 August 2021; accepted 7 September 2021)

ABSTRACT

Starting in mid-November, China was hit by several cold events during the early winter of 2020/21. The lowest temperature observed at Beijing station on 7 January reached −19.6°C. In this paper, we show that the outbreak of the record-breaking extreme cold event can be attributed to a huge merging Ural blocking (UB) ridge over the Eurasian region. The sea-ice cover in the Kara and East Siberia Seas (KESS) in autumn was at its lowest value since 1979, which could have served as a precursor signal. Further analysis shows that several successive UB episodes occurred from 1 September 2020 to 10 January 2021. The persistent UB that occurred in late September/early October 2020 may have made an important contribution to the October historical minimum of sea ice in the KESS region. Our results also show that, after each UB episode in winter, significant upward propagation of wave activity occurred around 60°E, which resulted in weakening the stratospheric vortex. Meanwhile, each UB episode also caused a significant reduction in sea-ice extent in KESS and a significant weakening of the westerly jet in mid–high-latitude Eurasia. Results suggest that the Arctic vortex, which is supposed to enhance seasonally, became weaker and more unstable than the climatic mean under the seasonal cumulative effects of UB episodes, KESS warming, and long-lasting negative-phase North Atlantic Oscillation (NAO–). Those seasonal cumulative effects, combined with the impact of La Niña winter, led to the frequent occurrence of extreme cold events.

Key words: extreme cold events, Ural blocking, Arctic sea ice, Arctic vortex, cumulative effect

Citation: Yao, Y., W. Q. Zhang, D. H. Luo, L. H. Zhong, and L. Pei, 2022: Seasonal cumulative effect of Ural blocking episodes on the frequent cold events in China during the early winter of 2020/21. *Adv. Atmos. Sci.*, **39**(4), 609–624, https://doi.org/10.1007/s00376-021-1100-4.

Article Highlights:

- The sea-ice cover in the Kara and East Siberia Seas in autumn 2020 was at its lowest value since 1979, which provides a precursor signal.
- Successive Ural blocking (UB) episodes that occurred from fall 2020 to January 2021 served as crucial physical processes.
- The seasonal cumulative effects of UBs, combined with other abnormal factors, led to the frequent occurrence of extreme cold events.

1. Introduction

On 6 January 2021, China was impacted by the strongest cold air outbreak of that winter, accompanied by widespread strong cooling and windy weather. Several meteorological stations observed their lowest temperatures on record for the same period during 6–8 January. For example, the 2-m temperature recorded at Beijing station on 7 January reached −19.6°C, which is the second-lowest temperature since 1951 (http://www.cma.gov.cn/2011wmhd/2011wzbft/2011wftzb/202101/t20210107_569795.html). In addition, China also experienced several frequent cold events in the early winter of 2020/21.

In recent years, along with continued global warming and regional climate anomalies, extreme weather—espe-

※ This paper is a contribution to the special issue on Extreme Cold Events from East Asia to North America in Winter 2020/21.

* Corresponding author: Yao YAO
Email: yaoyao@tea.ac.cn

cially extreme cold weather in winter—has been frequently observed over continental Eurasia (Ding et al., 2008; Hui, 2009; Wu et al., 2011, 2017; Cohen et al., 2014; Yao et al., 2016, 2017) and North America (Whan et al., 2016; Cohen et al., 2018a). Extreme cold surges are an important research topic because they have a significant impact on many aspects of people's daily lives—for example, their clothing, food, housing, and economic activities. Many studies have examined the physical causes of such extreme weather processes (Ding et al., 2008; Hui, 2009; Wu et al., 2011, 2017; Luo et al., 2014; Yao et al., 2017; Zheng et al., 2021). For the invasion of cold air from the Arctic to mid–low-latitude land areas, anomalous meridional circulation is necessary to provide a suitable background such as blocking and a negative-phase of the North Atlantic Oscillation (NAO–) (Herring et al., 2016; Whan et al., 2016; Yao et al., 2016; Martineau et al., 2017). The meridional circulation can guide the southward movement of cold air in the polar regions and is the conceptual equivalent to opening a gap through the strong westerly jet. In addition, a climatic context is necessary for such extreme anomalous meridional circulation to occur—for example, ENSO, Arctic amplification, etc. (Ding et al., 2008; Hui, 2009; Wu et al., 2011; Yao et al., 2017; Zheng et al., 2021). In other words, the occurrence of an extreme weather process is often the result of a combination of several factors (Yao et al., 2016, 2017; Li et al., 2020; Zheng et al., 2021).

Many studies (Luo et al., 2016; Gong and Luo, 2017; Chen et al., 2018; Tyrlis et al., 2019) have examined the important role of Ural blocking (UB) in driving Arctic sea-ice loss and Eurasian cold extremes and their link with the stratospheric vortex in autumn and early winter 2016-17 (Tyrlis et al., 2019). Large-scale atmospheric circulations such as UB and the Siberian high may increase the frequency of cold waves over Eurasia by intensifying the amplitude of the westerly jet meandering under the forcing of global warming, as revealed by Ma and Zhu (2019). Lü et al. (2020) suggested that the accumulation of snow in Siberia can contribute to sudden stratospheric warming and its downward transmission, which in turn facilitates the formation and development of a negative phase of the NAO, ultimately causing the onset of extreme cold weather in Eurasia. Zhang et al. (2019) suggested that the dipole mode of Eurasian winter-spring snow cover can induce large-scale teleconnection patterns by influencing sea-ice concentrations (SICs), thus further prolonging the cold conditions in Eurasia. The link between Arctic amplification and mid-latitude extreme cold weather in the context of global warming has become a hot topic of research (Cohen et al., 2014; Wu et al., 2015, 2017; Overland et al., 2016; Francis et al., 2017; Wu, 2017). Many studies have examined how anomalies in pre-existing sea ice can affect the state of atmospheric circulation (Gong and Luo, 2017; Wu, 2017; Chen et al., 2018) or precipitation in later periods, and on time scales that are likely to be cross-seasonal (Li and Wang, 2012; Wu et al., 2017; Han and Li, 2018; Li et al., 2018; Lü et al., 2019; Ding et al., 2021). Han and Li (2018) indicated that the sea-ice anomaly in the Labrador Sea in winter seems to be a better precursor for predicting the spring precipitation anomalies over southeastern North America and Western Europe. Several authors have published detailed reviews on Arctic sea ice and its possible link with Eurasian climate, from which we can see that the possible link between sea ice in the Arctic and atmospheric circulation is a consistent assertion, but that controversies also still exist (Gao et al., 2015; Cohen et al., 2018b). Indeed, due to the uncertainties and chaotic nature of the atmosphere and other systems, research in this area is still very challenging, and the resultant academic debate is ongoing (Wu et al., 2017; Dai and Song, 2020).

In any case, the extreme cold surges affecting the Eurasian midlatitudes are very closely related to meridional circulation anomalies (such as blocking). Although most cold surges have certain commonalities, each individual case is unique given the nonlinear and chaotic nature of the atmosphere. This uniqueness is what makes related in-depth investigations a continually worthwhile pursuit. In fact, in many cases, extreme weather events are dominated by one kind of weather process but at the same time require the involvement of other weather systems. For instance, Yao et al. (2016) proposed a mechanism for the combined effect of the NAO and European blocking on extreme snowstorms in Europe. In addition, their latest study highlights the unique combined effect of the NAO and European blocking on European heat waves (Li et al., 2020). As mentioned in these studies (Luo et al., 2015; Yao et al., 2016; Li et al., 2020), the combined effect of the NAO and blocking circulation mainly manifests as the NAO changing the position and shape of the downstream blocking by altering the strength, orientation, and position of the westerly jet. In addition, the ways in which the processes of the two systems can combine to impose a collective effect can be both spatial and temporal in form, and then possibly involve atmospheric teleconnection processes. In the case of a temporally combined process, the time scale may extend from a contemporaneous one to an interseasonal, interannual, or even an interdecadal one. This study examines the specific physical processes involved in this cold event and the possible combined effect that existed within these processes.

The remainder of this paper is structured as follows: The datasets and methods are described in section 2. In section 3 we describe the evolution of the atmospheric circulation during the January 2021 cold event and its detailed features from a daily perspective. The historical minimum value of the sea ice in the Kara and East Siberia Seas (KESS) in autumn (October) 2020 is investigated in section 4, which is considered as a precursor to this cold event. Also in section 4, we show how the UB was organized into five successive events from 1 September 2020 to 6 January 2021. Meanwhile, the upward flux of wave activity induced by the UB can weaken the stratospheric vortex. The anomalies of the West Pacific sea surface temperature (SST) associated with La Niña are presented in section 5. Finally, conclu-

sions and some further discussion are provided in section 6.

2. Data and methods

2.1. *Datasets*

The main datasets used in this study are the latest daily reanalysis (ERA5) dataset (Hersbach and Dee, 2016) from the European Centre for Medium-Range Weather Forecasts, covering the period from 1979 to 2021 and including geopotential height, temperature, horizontal wind components (u and v), surface (2-m) air temperature (SAT), surface pressure, and SIC, at a 2.5° × 2.5° spatial resolution, and the monthly SIC and SST data derived from the Met Office Hadley Centre at a resolution of 1° × 1°. To corroborate the robustness of the sea-ice variability, the monthly and daily (1 September 2020 to 1 January 2021) datasets of the National Snow & Ice Data Center (NSIDC) in the northern polar stereographic projection, on a grid of 25 km × 25 km, are also used in this paper.

To measure the SAT variability over the region of China under the impact of the cold event, the time-mean (1–8 January 2021) temperature data of 2414 stations nationwide are used, as well as the mean temperature data of nationwide stations from 1 September 2020 to 1 January 2021. Furthermore, the monthly tropical SST series, including the Niño-1+2, Niño-3.4, and Niño-4 indexes, and the daily NAO index, from the Climate Prediction Center (https://psl.noaa.gov/data/climateindices), are used to examine the impact of multi-factor synergy on this cold-air outbreak over East Asia.

2.2. *Methods*

The occurrence of this cold event was closely related to the UB, and so it is necessary to examine the evolution of the UB during this period. To prevent omitted UB cases, two kinds of identification methods are used in this research, the geopotential height anomaly, and the one-dimensional blocking index (Tibaldi and Molteni, 1990), abbreviated as TM index. A UB case is defined when at least one of these two conditions is met. Specifically, the first method works based on the maximum value of the 500-hPa geopotential height anomaly over the region (40°–85°N, 30°–150°E) being larger than 250 gpm for at least five consecutive days. The TM index method, meanwhile, refers to the reverse of the 500-hPa geopotential height gradient, which is defined by

$$\mathrm{GHGN} = [Z500(\lambda,\phi_N) - Z500(\lambda,\phi_0)]/(\phi_N - \phi_0)\,,$$

$$\mathrm{GHGS} = [Z500(\lambda,\phi_0) - Z500(\lambda,\phi_S)]/(\phi_0 - \phi_S)\,,$$

where Z500 indicates the 500-hPa geopotential height, $\phi_N = 80°\mathrm{N} + \Delta$, $\phi_0 = 60°\mathrm{N} + \Delta$, $\phi_S = 40°\mathrm{N} + \Delta$, and $\Delta = -5°$, 0° or 5°. A UB case can be recognized if two criteria, GHGS > 0 gpm $(°\mathrm{lat})^{-1}$ and GHGN < −10 gpm $(°\mathrm{lat})^{-1}$, are both met for at least 10 consecutive longitudes (λ) and five continuous days within the zonal range of 30°–150°E. Lag-0 is the strongest day of the UB, which denotes when the maximum value of the geopotential height anomaly is at its largest during the lifespan of the UB.

To explore the spatial distributions of the cold air mass and its source during this cold event, according to Iwasaki et al. (2014), the cold air mass (DP) is given as the pressure difference between the earth's surface and the isentropic surface of a reference potential temperature (θ_T), $\mathrm{DP} = P_\mathrm{S} - P(\theta_\mathrm{T})$, where P_S and $P(\theta_\mathrm{T})$ signify the pressure of the earth's surface and a specific isentropic surface separately. $\theta_\mathrm{T} = 280\,\mathrm{K}$, as in Iwasaki et al. (2014). The temporal evolution of the local cold air mass can be expressed as $\partial(\mathrm{DP})/\partial t = -\nabla\cdot\boldsymbol{F}_\mathrm{C} + Q$, where Q signifies the variability of potential temperature due to diabatic heating (Yamaguchi et al., 2019). $\boldsymbol{F}_\mathrm{C} = \int_{P(\theta_\mathrm{T})}^{P_\mathrm{S}} \boldsymbol{v}\mathrm{d}p$ is the cold air mass flux and $\mathbf{v}$ is the horizontal wind vector.

During this cold air outbreak, the stratospheric and tropospheric polar vortices weakened and split, and variabilities in the stratosphere were consistently caused by the upward tropospheric signal. For this purpose, the Eliassen-Palm (EP) flux in spherical geometry can be calculated to depict the impact of tropospheric planetary-scale activity on the stratosphere. The EP flux, $\boldsymbol{F} = (F_\varphi, F_p)$, can be written as $F_\varphi = -R\cos\varphi\overline{u'v'}$, $F_p = Rf\cos\varphi\overline{v'\theta'}/\theta_p$ (Edmon et al., 1980), in which R, f, φ and θ are the Earth's radius, Coriolis parameter, latitude, and potential temperature, respectively. Overbars signify the zonal mean over a given zonal range, and primes signify departures therefrom. The transformed mean zonal equation can be obtained as $\partial\bar{u}/\partial t = (R\cos\varphi)^{-1}\nabla\cdot\boldsymbol{F} + f\,\bar{v}^*$, where $\bar{v}^*$ is residually meridional circulation (Andrews and McIntyre, 1978). In this paper, the daily tendency of zonal wind caused by the variance of the EP flux can be expressed as $\Delta\bar{u} = \{(R\cos\varphi)^{-1}\nabla\cdot\boldsymbol{F}\}\Delta t$, Δt = 1 day. Given that F_p cannot display the spatial distributions of upward wave energy, the poleward eddy heat transport (EHT) $v'T'$ at 100-hPa can therefore be used to diagnose the horizontal distribution of EP between the stratosphere and troposphere (Tyrlis et al., 2019). The value of EHT corresponds well to F_p, wherein a positive value denotes the upward propagation of wave energy from lower levels.

3. Extreme cold weather event in January 2021

3.1. *Evolution of the atmospheric circulation*

On 6 January 2021, China was hit by a widespread cold wave accompanied by strong cooling and windy weather. Figure 1 shows the SAT anomaly distribution averaged from 6 to 8 January based on the station-observed data (2414 stations). It can be seen that nearly all of China experienced a sharp SAT decline during 6 to 8 January, except for a small part in southwestern China. The average SAT in northern China from 6 to 8 January was more than −10°C colder

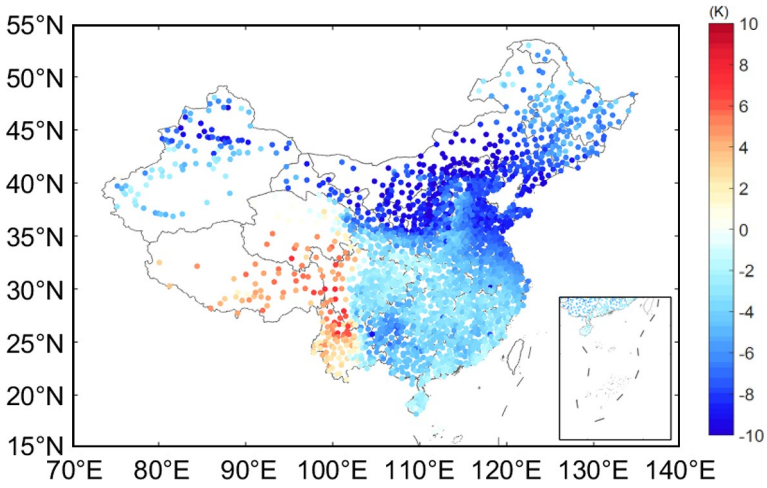

Fig. 1. Spatial patterns of time-averaged (6–8 January 2021) SAT anomalies (units: K) relative to corresponding daily means for 1981–2010 of 2414 stations across China.

than climatology. Even over the most southern region of China, the SAT still exhibited a clear decline during this cold wave. To visualize the physical processes during this cold event, it is necessary to examine the evolution of the atmospheric circulation, especially from the daily perspective. Figure 2 shows the daily evolution of the geopotential height at 500 hPa and the SAT anomalies from 29 December 2020 to 9 January 2021. On 29 December, a huge anticyclone already existed over mid–high-latitude Eurasian land areas, which can be identified as a UB process. It can be seen that the anticyclonic center covered a large area from around 0° to 120°E, with the maximum center located at approximately 60°E. The cyclonic center located to the southeast of the anticyclone was much weaker in intensity compared to the anticyclonic center. However, the anticyclonic center had a southward spread around 30°E to 60°E and reached 30°N on 4 January and even to 30°N on 9 January (Fig. 2). This may have been due to the mid–low-latitude wave train that developed from 29 December to 9 January. Starting from 29 December, we can see that there was a latitudinal wave train starting to develop from the North Atlantic to the Mediterranean Sea, which then extended to near the Caspian Sea. The wave train had a structure, and the last positive center of the wave train was the part of the UB anticyclonic center that extended southward during this period. In other words, the wave train and the UB both developed in the same period, and some parts of the two merged and coupled together during their development.

Therefore, there were quite a few differences between this UB (Fig. 2) and the classical UB structure described in previous observational studies (see Fig. 8b in Yao et al. (2017)). In the North Atlantic region, the latitudinal wave train mentioned above had an unstable structure during its development from 29 December to 9 January (Fig. 2). From 2 to 9 January, the positive and negative anomaly centers over the North Atlantic region gradually shifted from a latitudinal to a longitudinal orientation and developed into a northwest–southeast-tilted dipole mode (Fig. 2). This dipole mode had a classic NAO− structure as shown in many previous studies (e.g., Benedict et al., 2004; Yao and Luo, 2014), only at a lower overall latitude than the mean state. An NAO in a more shifted mean state will have a different impact on the local weather, leading to an increased probability of extreme weather processes (Yao and Luo, 2014; Yao et al., 2016; Li et al., 2020). In fact, the defining criterion for an NAO or blocking event is the unified description standard for their most common characteristics. However, each individual case has its own deviations from this criterion. At the same time, each individual case is likely to be accompanied by other systems when it occurs, and such deviations and combined impacts between systems are probably the most important nonlinear and uncertain mechanisms leading to the occurrence of extreme weather, as revealed by previous research (Luo et al., 2015; Yao et al., 2016; Li et al., 2020). The collective processes during this cold event are further described in section 5.

Meanwhile, the positive and negative SAT anomalies that accompanied the UB geopotential height anomalies can also be examined (Fig. 2, shading). It can be seen that positive (negative) geopotential height anomalies were associated with positive (negative) SAT anomalies, which is the classical characteristic of temperature distribution due to blocking circulation as presented in previous studies (Luo et al., 2016; Yao and Luo, 2018). The positive SAT anomaly at high latitudes around the KESS region would have favored a decline in sea ice during the UB life cycle on the synoptic time scale (Luo et al., 2017), which is demonstrated in the following section. As the blocking developed, the negative SAT anomaly associated with the cyclonic center, shown in Fig. 2, moved slowly from the Siberian region to the middle and lower latitudes, eventually causing significant cooling to occur in areas of east-central and southern China on 6 January. In fact, from the end of December to the 8th of January, China experienced two extreme cold

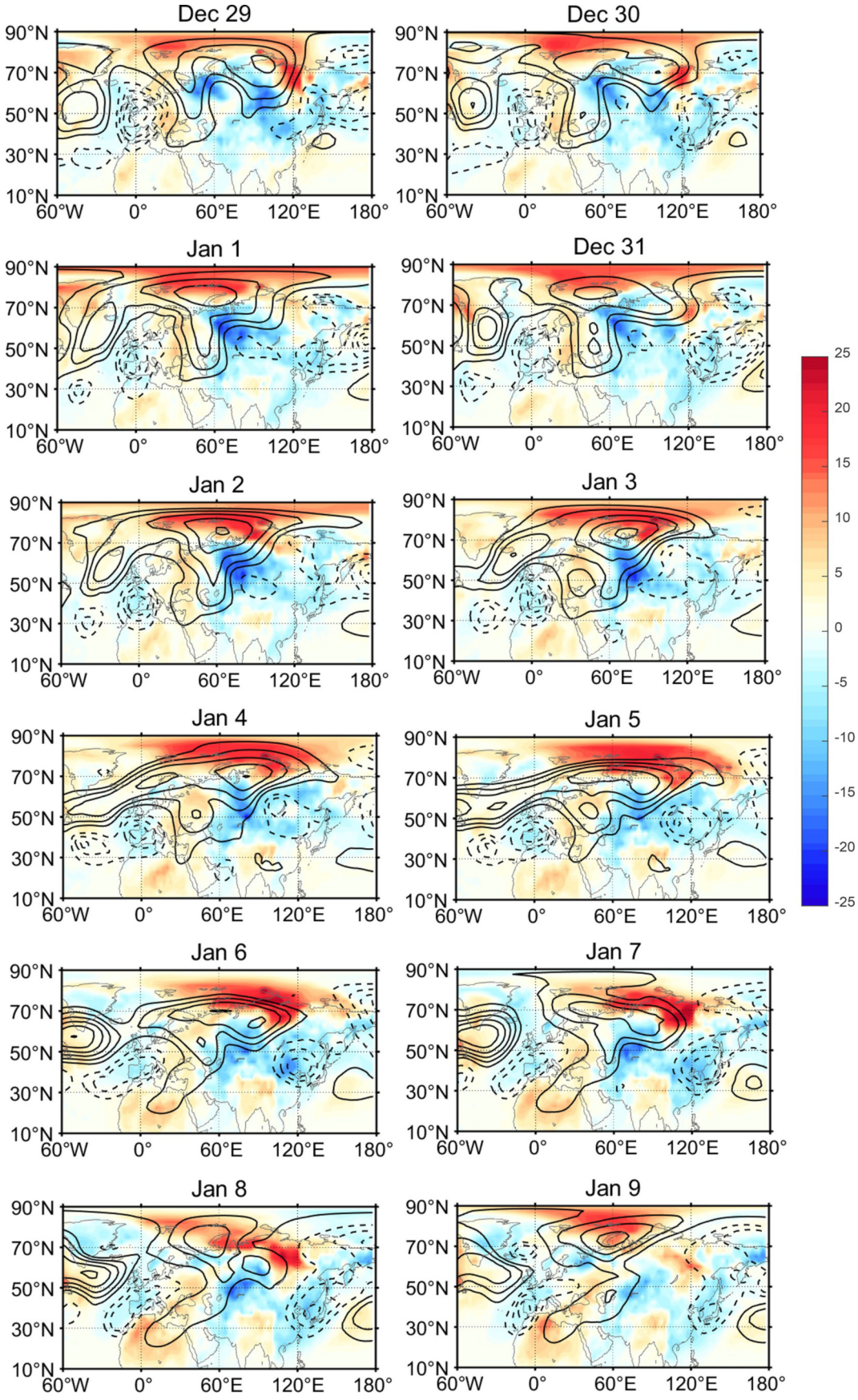

Fig. 2. Evolutions of daily spatial distributions of 500-hPa geopotential height (contours, CI = 80 gpm) and SAT (shading, units: K) anomalies from 29 December 2020 to 9 January 2021.

events, which has been indicated by Zheng et al. (2021). This will be mentioned later in the further analysis.

3.2. *Source and pathways of the cold air*

To provide a more visual representation of the origin of this cold air and its pathways, we calculated the cold air flux to show the movement of the cold air mass in Fig. 3. It can be seen that at the end of December the source of the cold air (shaded in red) was over the Arctic, at around 120°E. Then, beginning on 1 January, the cold air started to

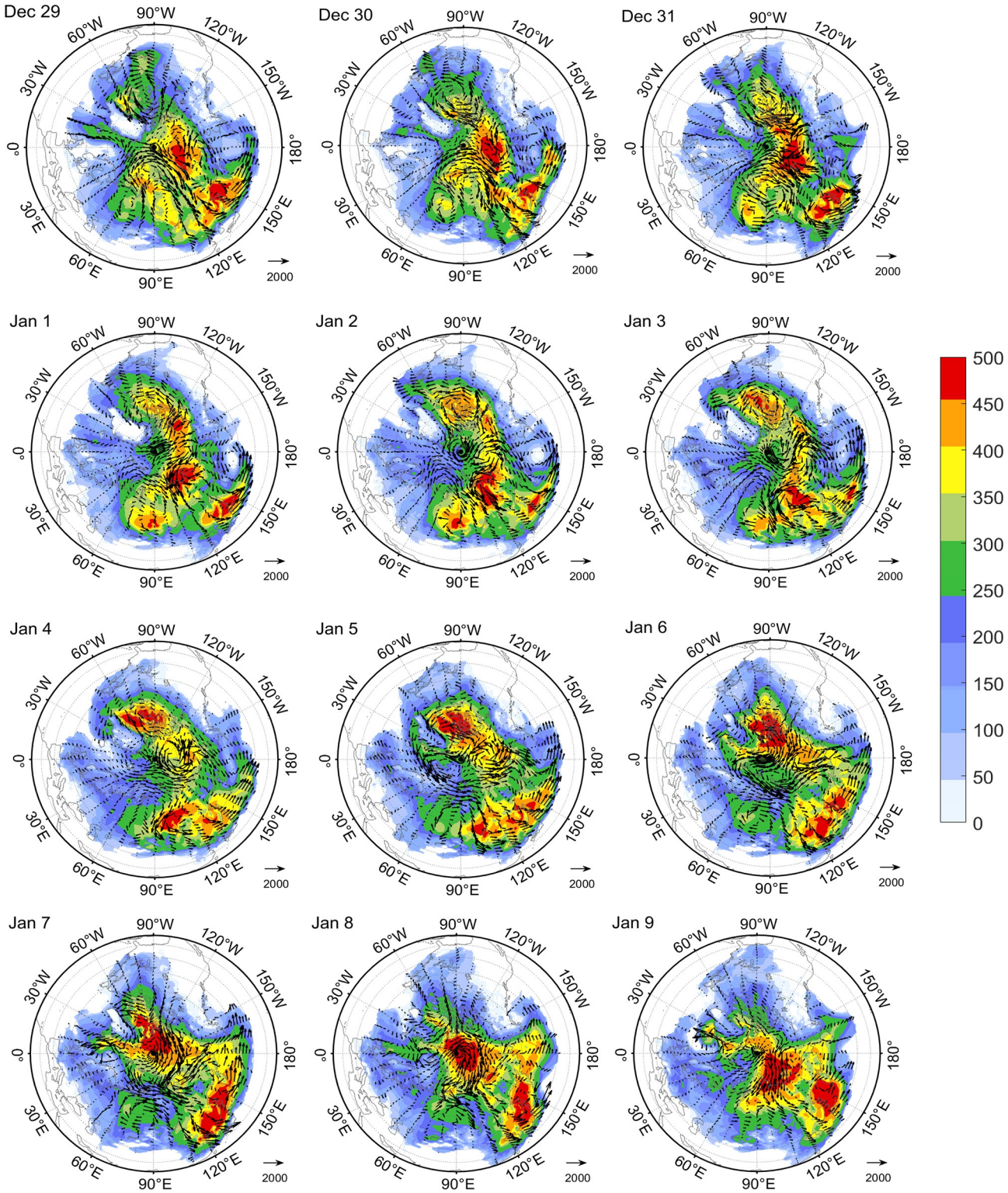

Fig. 3. Spatial patterns of daily cold air mass (shading; in hPa) and its flux vector (arrows; in hPa m s^{-1}) from 29 December 2020 to 9 January 2021. Cold air mass, $\mathrm{DP} = P_S - P(\theta_T)$, is defined as the pressure difference between the 280-K potential temperature surface $P(\theta_T)$ and the earth's surface P_S, and its flux vector can be expressed as $\int_{P_S}^{P(\theta_T)} \boldsymbol{v}\mathrm{d}p$, $\boldsymbol{v} = (u, v)$.

move gradually towards the lower latitudes. The direction of movement of the cold air can be observed through the wind vectors (arrows) in Fig. 3. By 3 January, the cold air had moved pointedly into the middle and high latitudes and was distributed between 90° and 120°E. Then, from 5 January onwards, the cold air mass split from the higher latitudes and moved rapidly to the middle and lower latitudes. From 6 to 9 January, it can be seen that a large, relatively independent cold air mass had emerged at 120°E in the middle and low latitudes. This cold air mass was entrenched over the central-eastern and southern parts of China, causing an outbreak of extremely cold weather as shown in Fig. 1. It should be pointed out that on 29 December 2020, a strong mass of cold air had settled over northeast China, which caused a prominent cooling process to take place over a wide area of the country. In other words, about a week before this extreme cold event (6 Jan), an appreciable cooling process had already been experienced by most of China, therefore, this extreme cold wave was preceded by the combined impacts of at least one or even a few cold waves. Several cooling processes were closely associated with the UB, and these coactive processes are examined in detail together in section 5.

4. Signals of pre-autumn KESS sea ice

To investigate the potential role of the Arctic sea-ice anomaly on the cold event, we show the sea-ice cover distributions for each month in autumn 2020 in Fig. 4. To avoid uncertainty between different datasets, two widely used sea-ice datasets (Hadley sea-ice data and the NSIDC dataset) were used simultaneously. The data suggest that, for the entire Arctic, the negative sea-ice cover anomaly was mainly concentrated in the KESS (75°–85°N, 60°E–180°) for each month in autumn. The negative sea-ice anomaly was most evident in October during autumn 2020. The negative sea-ice anomaly in autumn may have caused a weakening of the meridional temperature gradient in the middle and high latitudes of the Eurasian region, causing the westerly jet to weaken and become unstable in the Eurasian region, providing a favorable background condition for the excitation of future meridional circulation anomalies, as revealed in Tyrlis et al. (2019). It can be seen that the negative anomaly of the sea ice moved gradually from the KESS (Figs. 4b and e) towards the Barents–Kara Seas as the season became colder (Figs. 4c and f).

To determine whether the sea-ice cover in KESS in autumn 2020 was extremely low compared to historical val-

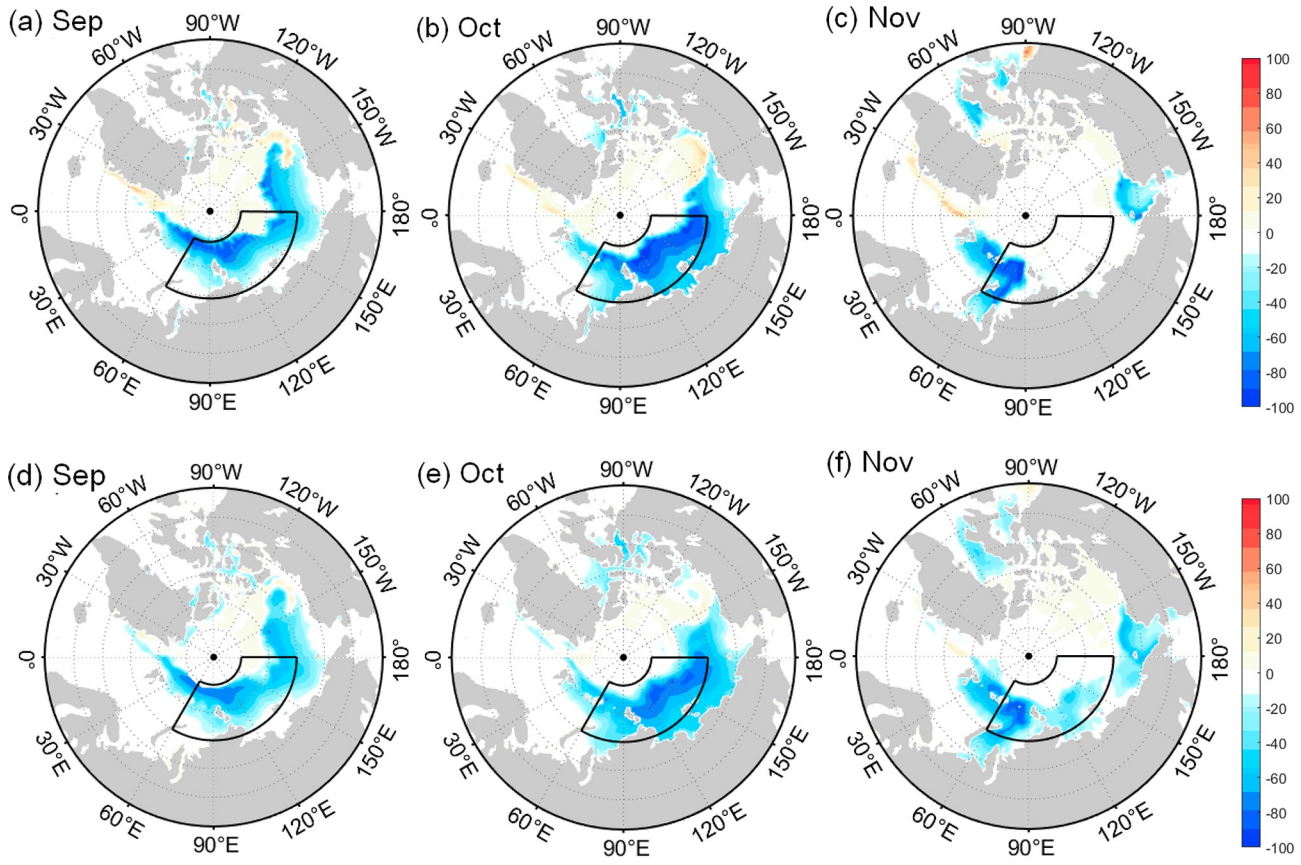

Fig. 4. Spatial patterns of SIC anomalies (units: %) for (a, d) September, (b, e) October, and (c, f) November 2020, based on monthly SIC data from (a–c) the Met Office Hadley Centre and (d–f) NSIDC. The region marked by the black frame is KESS (75°–85°N， 60°E–180°).

ues, we present the Arctic sea-ice variabilities from 1979 to the present day in Fig. 5. Figures 5a and c show the variabilities of sea-ice cover in the entire Arctic for autumn (and each month of autumn). It can be seen that the autumn sea-ice cover in the entire Arctic has been decreasing rapidly since 1979, due to the effects of Arctic amplification (Figs. 5a and c). The Arctic sea-ice cover in September reached its lowest value on record in 2012 as shown in Figs. 5a and c (red dashed lines), which is consistent with the associated official report (https://www.nasa.gov/topics/earth/features/2012-seaicemin.html). In addition, it can be observed that the Arctic sea-ice cover in October 2020 (blue dashed lines) reached its lowest value on record since 1979. Although the Arctic sea-ice cover in autumn 2020 was very close to that of 2012 (Hadley) and 2016 (NSIDC), it was also numerically at its lowest level on record since 1979. Thus, the extremely low sea-ice anomaly in the Arctic may have provided a pre-existing signal for the atmospheric circulation to act upon in later months. However, for the Eurasian region, the sea ice in the KESS may have a closer link with the atmospheric circulation and extreme weather, according to previous studies (Luo et al., 2016, 2017; Tyrlis et al., 2019). Therefore, we show the KESS sea-ice variabilities since 1979 in Figs. 5b and d. The results show that the KESS sea-ice cover in both October and autumn 2020 exhibited their lowest recorded values since 1979. In particular, the KESS sea-ice cover in October 2020 (blue dashed lines in Figs. 5b and d) was well below the second-lowest value on record. In summary, the conclusion that the KESS sea-ice cover in October and autumn 2020 were at their lowest values since 1979 is solid and reliable, both for the Hadley and NSIDC sea-ice datasets. In the following section, we discuss several crucial processes that preceded the cold event on a cross-seasonal time scale and then identify their combined effects.

5. Combined effects of UB and other climatic factors

5.1. *Cumulative effects of several consecutive and persistent UBs*

It has already been mentioned above that UBs exert an important influence on Eurasian temperatures and KESS sea-ice changes. Therefore, it is necessary to examine the frequency of UBs from autumn 2020 to January 2021. We identified five UB episodes using the identification method mentioned earlier from 1 September 2020 to 16 January 2021, as shown in Fig. 6a (gray shading). From mid-November to January 2021, three consecutive UB episodes occurred with only a few days between each episode. The Ural regional mean 300-hPa zonal wind exhibited frequent fluctuations from 1 September to 16 January (red solid line in Fig. 6a). This suggests that each UB episode contributed significantly to the weakening of the westerly zonal wind on synoptic time scales. The onset of a UB, accompanied by the establishment and strengthening of the meridional circulation, would inevitably have led to a weakening of the mid- and high-latitude regional zonal wind (Luo, 2005; Luo and Cha, 2012; Yao et al., 2017). The regional mean climatic zonal wind, as shown in Fig. 6a (dashed line), slowly strengthened from the warm to the cold season. However, due to the seasonal cumulative effect of consecutive UB episodes, the zonal wind during mid-November to January became unstable and weakened dramatically, to a level much lower than the climatic mean. The weakening of the

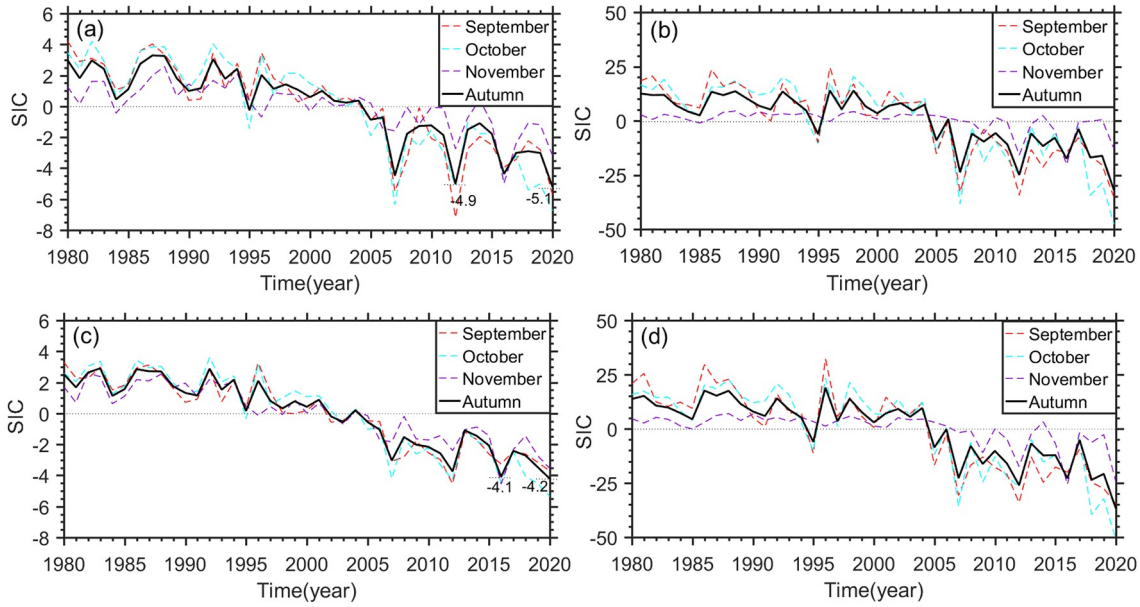

Fig. 5. Time series during 1980–2020 of the spatially averaged SIC anomaly (units: %) over (a, c) the whole Arctic and (b, d) KESS (75°–85°N, 60°E–180°). The red, blue, and purple dashed lines represent the SIC variations in September, October, and November, respectively, and the black solid line represents the autumn mean. The monthly SIC dataset used here is derived from (a, b) the Met Office Hadley Centre and (c, d) NSIDC.

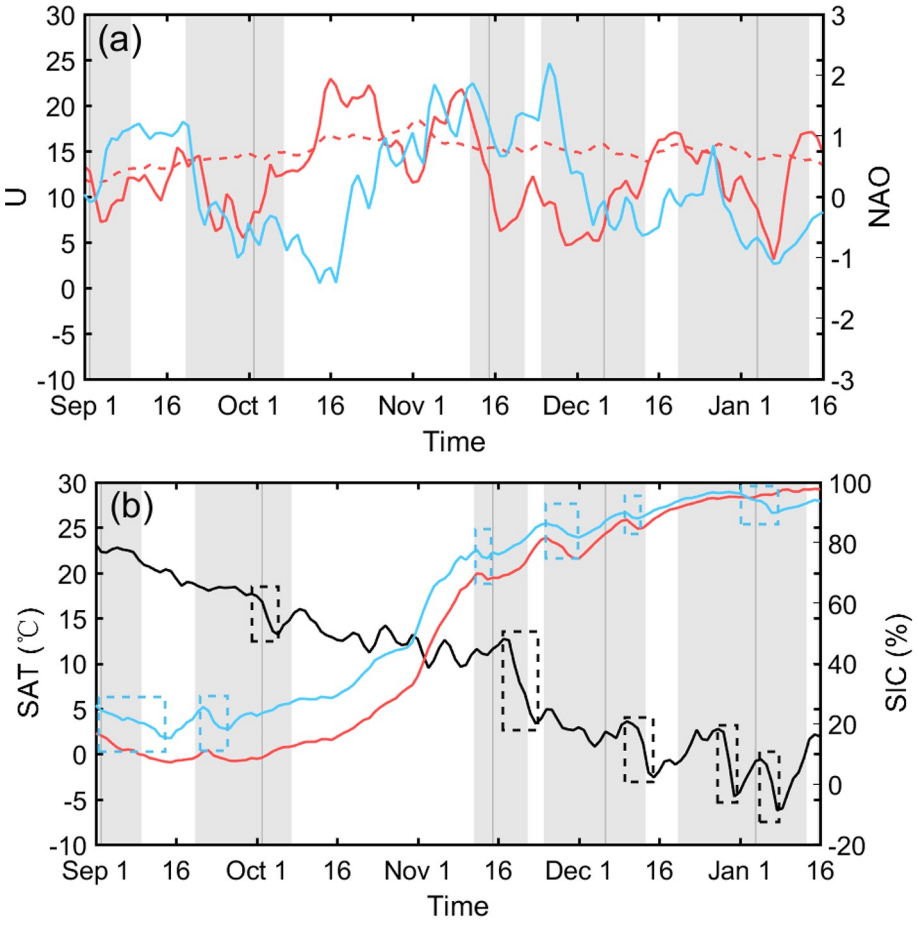

Fig. 6. Time series of (a) the 300-hPa zonal wind (units: m s^{-1}) averaged over the Ural region (45°–65°N, 30°–120°E), where the red solid line represents autumn/winter 2020, the red dashed line represents the corresponding daily mean during 1980–2020, and the blue line is the normalized NAO index, (b) the KESS (75°–85°N, 60°E–180°) SIC derived from the monthly data of NSIDC (red line) and ERA5 (blue line) and mean SAT of 2414 stations nationwide (black line). The black (blue) dashed boxes indicate the sharp SAT (SIC) decline associated with UB. The gray shading represents the UB episodes and the vertical gray line represents the Lag-0 day for each UB episode.

high-altitude zonal jet would have affected the stability of the polar vortex and changed the normal seasonal strengthening process of the polar vortex from autumn to winter (Tyrlis et al., 2019). This may have provided the background conditions for the early jet stream dynamics to change and eventually allow for the cold wave outbreak in early January. In addition, the NAO daily index is also plotted in Fig. 6a (blue line), from which a clear positive NAO episode (NAO+) can be observed before or at the beginning of each UB episode (gray shading). This is consistent with previous findings that outlined the physical mechanism whereby a NAO+ episode favors the development of a downstream UB (Luo et al., 2016; Yao et al., 2017; Yao and Luo, 2018). At the same time, the development of NAO+ episode usually occurs a few days ahead of blocking over Europe (Yao and Luo, 2018). We further composite the NAO and UB index based on the peak day of the four UB episodes and calculate the lead-lag correlation between them (not shown). Results show that the transition of the NAO to its positive phase typically occurs 10 days ahead of a UB episode with a correlation coefficient of 0.78, which also confirms the conclusion mentioned above that each UB is preceded by a NAO+ episode. Here, the NAO index had been negative in value since the start of December, and, although there was a brief positive phase at the end of December, it turned negative again immediately thereafter. This may be attributed to the frequent UB episodes that began in mid-November and the associated weakening of the westerly jet mentioned above. Three consecutive and long-lasting UBs provided favorable westerly jet conditions for the NAO to change from positive to negative phase and to be maintained over a long period. At the same time, the positive feedback (Luo and Cha, 2012; Yao and Luo, 2018) of the NAO− contributes to a notable weakening of the mid-to-high-latitude westerly jet in the North Atlantic and western Europe. We also composite the UB index and regional (Eurasian region) mean 300-hPa zonal wind based on the peak day of the four UB episodes (not shown). Results show that a UB occurs three days

ahead of the Ural regional mean 300-hPa zonal wind with a correlation coefficient of –0.69. Thus, the seasonal cumulative and combined positive feedbacks of the NAO– and a UB will contribute to a weakening of the mid-to-high-latitude westerly jet across the North Atlantic and Eurasian region, providing favorable conditions for the merger and development of the large-scale anomalous meridional circulation illustrated in Fig. 2.

Figure 6b shows the variations of the KESS sea ice and SAT over China. The station-observed SAT showed a normal seasonal decline from autumn to winter (black line in Fig. 6b); and within this seasonal change, four instances of dramatic SAT decline can be observed during each UB episode, which were closely linked to the frequent occurrence of cold events during early winter of 2020/21. Three significant SAT declines before 6 January set the stage for the record low temperatures on that day. The physical mechanisms related to the UB, which plays an important role in SAT declines in East Asia, especially in China, have been examined in previous studies (Yao et al., 2017; Tyrlis et al., 2019). In addition, when a UB occurs, it causes significant warming to occur at high latitudes, particularly in the Barents–Kara Seas, which causes rapid melting of sea ice on synoptic time scales (Luo et al., 2016, 2017; Tyrlis et al., 2019). In this study, however, we are concerned with the KESS region, which partially overlaps with the Barents–Kara Seas, but is a little further east and contains the East Siberian Sea. This is because the sea-ice anomalies in Figs. 4 and 5 were in the KESS region. In addition, the location of this UB episode was higher in latitude relative to the climatic norm and more extensive, so the extent of impact was different. The variation of KESS sea ice from 1 September to 16 January is shown in Fig. 6b (red and blue lines). Sea-ice coverage gradually increased as the seasonal decline in temperature in KESS progressed from September to January. Then, amid the gradual increase in KESS sea ice, there were six relatively significant short periods of decline (blue boxes), as shown in Fig. 6b. Each of these short-term reductions in KESS sea ice was accompanied by a UB episode. A UB had a more pronounced effect on the reduction in sea ice in the Barents–Kara Seas during this period (not shown). However, because the abnormal signal of sea ice in the early autumn was concentrated in the KESS region, we focus on the KESS region in this study. The data suggest that, from 1 to 16 September, accompanied by the seasonal reduction in KESS sea ice, the UB episode also made an important positive feedback to the sea-ice decline. In addition, the notable short-term sea-ice reduction during 20–26 September, due to the UB episode, may have been the main reason for the historical sea-ice minimum in KESS. In any event, several UB episodes made an important contribution (positive feedback) to the reduction in sea ice in the KESS region.

5.2. *Upward signals caused by UBs*

Several UB episodes preceding the onset of the record-breaking cold event not only caused a reduction in KESS sea ice and weakened the regional westerly jet, but may also have affected the stratosphere through modulating the upward progress of planetary-scale waves (Kodera et al., 2013; Shen et al., 2020), which in turn affected the stability of the polar vortex. Given that the meridional EHT $v'T'$ is directly proportional to the vertical component of the EP flux, we, therefore, show the horizontal distribution of EHT $v'T'$ at 100 hPa in Fig. 7 to explore the vertical propagation of wave energy associated with several crucial UB episodes. The results show that, during or after each UB episode, a significant positive (upward) EHT could be observed over the Ural region (near 60°E to 90°E), especially the UB episode that occurred in January 2021. This suggests that UB events can play an important role in the upward propagation of EP fluxes from the troposphere to the stratosphere over the Ural region. Meanwhile, anomalous signals of EP fluxes in the stratosphere are often followed by a UB by a few days to a week, as indicated in Fig. 8a (contours). We composite the

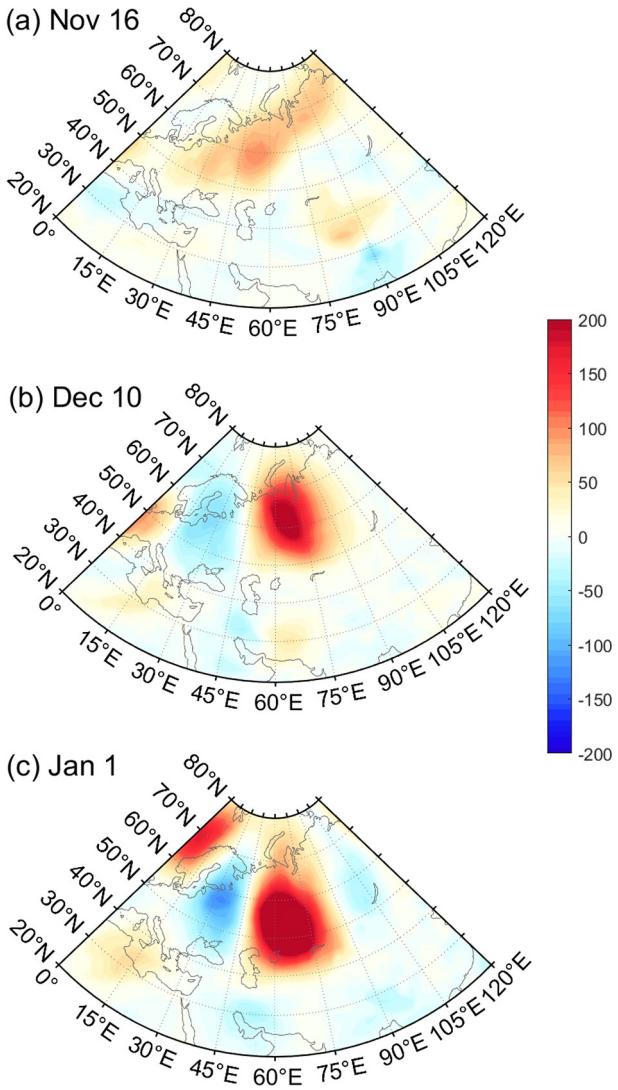

Fig. 7. Horizontal patterns of v_aT_a (units: K m s^{-1}) at the 100-hPa pressure level for (a) 16 November 2020, (b) 10 December 2020, and (c) 1 January 2021.

associated blocking index and F_p based on the peak day of the four UB episodes (not shown). The lead-lag correlation indicated that UB is ahead of F_p by five days with a correlation coefficient of 0.77. We also calculated the lead-lag correlation between them for the entire period from 1 September to 16 January. Results show that the UB is ahead of F_p by 5 days with a correlation coefficient of 0.6 (which is above the 90% confidence level based on a two-tailed Student's *t*-test). These results are consistent with related research (Tyrlis et al., 2019). Figure 8a shows the detailed vertical component of the EP flux, F_p at every vertical level, and the zonal wind tendency, $\Delta\bar{u}$, caused by the convergence or divergence of EP flux. The data suggest that the upward propagation of the EP flux caused by UB in October was not obvious (only up to 150 hPa). The upward EP flux due to the UB on 16 November was stronger than the former UB. Subsequently, two UB episodes in early December and January resulted in highly significant uploading of EP flux which penetrated up to the 10-hPa level, which then led to the strong aggregation of planetary-wave energy in the middle stratosphere, as shown in Fig. 8a. Meanwhile, the shading in Fig. 8a indicates the daily evolution of zonal wind tendency caused by the EP flux variance within one day. From mid-December 2020 to early January 2021, the stratosphere featured significant negative anomalies in zonal wind tendency associated with the upward propagation and stratospheric convergence of EP flux. Meanwhile, Fig. 8b shows the zonal mean *u*-wind anomaly at 55°N from autumn 2020 to January 2021. The data suggest that the notable upward propagation of EP flux (Fig. 8a) on 16 December and 1 January contributed greatly to the weakening of the upper-level (stratosphere) westerly jet and further weakened the zonal wind downward to the troposphere (as indicated by the arrow in Fig. 8b). The signal, which characterized the attenuated polar vortex in the stratosphere, penetrated down into the troposphere after 1 January to modulate the local weather over East Asia (Fig. 8b, arrows). This means that the UB episodes—especially the UBs that occurred during early December and January—markedly weakened the strength and stability of the polar vortex. The weakened polar vortex further stripped the cold air mass guided by the tropospheric UB, breaking up and peeling

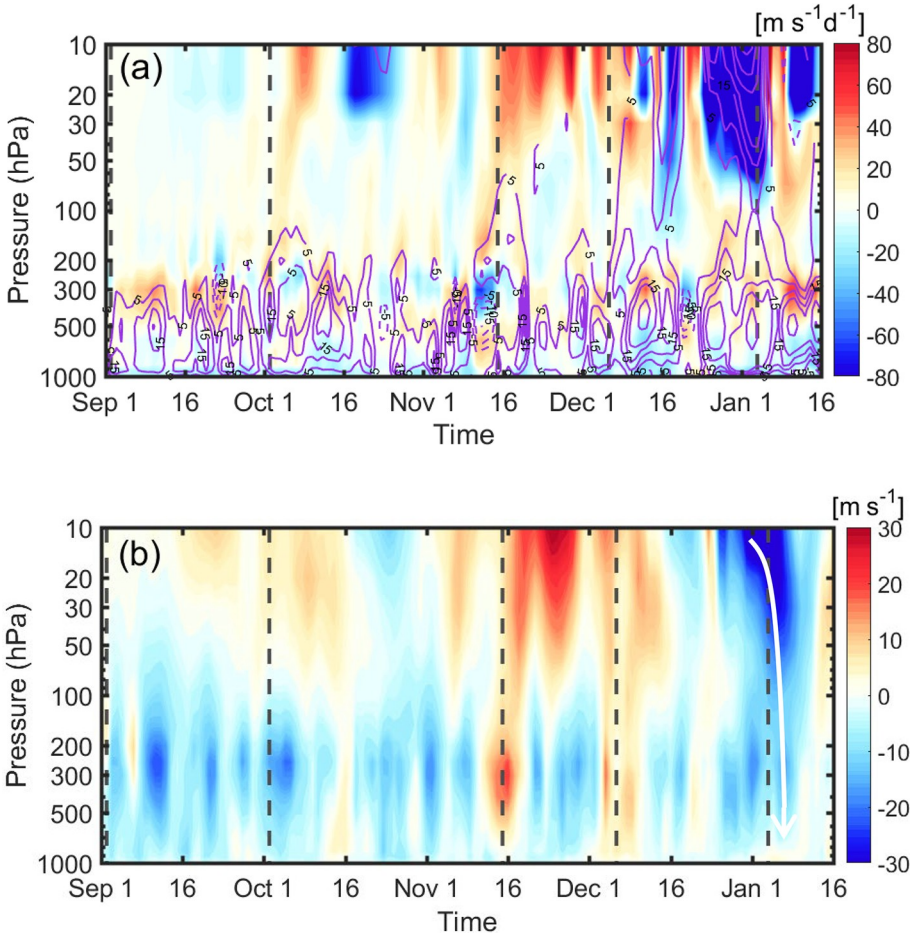

Fig. 8. Time–pressure evolutions of the (a) domain-mean (50°–80°N, 30°–120°E) zonal wind tendency (shading, units: m s^{-1} d^{-1}) and vertical component of EP flux (contours, × 10^6 m^2 s^{-2} Pa), and (b) zonal mean (90°–150°E) westerly wind anomaly at 55°N. Similar to Taguchi and Hartmann (2006), the variables in (a) are scaled by a factor inversely proportional to pressure $\sqrt{1000/P}$. The vertical dashed line represents the Lag-0 days of several UB events.

away from the main body, which in turn affected the middle and lower latitudes.

Finally, it is worth noting that the Pacific SST had been developing anomalously since the summer of 2020, which was a typical La Niña year (Zheng et al., 2021). The distribution of SST anomalies in the Pacific Ocean demonstrates a typical La Niña SST distribution (Fig. 9). The SST in the central-eastern equatorial Pacific shows a widespread negative anomaly, which contrasts sharply with the KESS warming (sea-ice decline) at high latitudes (Figs. 4 and 5). This contrast would have caused a weakening of the meridional temperature gradient in middle and high latitudes of Eurasia, favoring the development of a meridional circulation (i.e., a UB) (Yao et al., 2017; Tyrlis et al., 2019; Zheng et al., 2021). In addition, there may be anomalous oceanic or atmospheric signals that indirectly influenced the cooling processes of the 2020/21 winter. However, they will not be discussed in this study.

6. Conclusions and discussion

This paper focuses on the frequent occurrence of cold events during the early winter of 2020/21, in particular the record-breaking extreme cold event in early January in China. We have examined, in detail, the physical mechanisms of the processes involved (Fig. 10), mainly from the perspective of the large-scale atmospheric circulation (i.e., UB episodes in Fig. 10). At the same time, given the complex climatic background of this cold event, we have also explored other climatic factors that may have provided an abnormal background for these processes. In short, the historical minimum value of sea-ice cover in the KESS region that occurred in autumn was a pre-existing background condition, and several UB episodes from autumn to winter were specific seasonal cumulative physical processes (as indicated in Fig. 10, dashed lines and arrows). In addition, anomalously cold SSTs in the central-eastern Pacific due to an established La Niña, and a long-lasting NAO− event, were also important general background conditions. The seasonal cumulative and combined impacts (Fig. 10) of these processes led to the occurrence of these extreme cold events.

The sea-ice cover across the entire Arctic was at a historic minimum value (since 1979) in autumn 2020 (especially in October). The spatial distribution of sea ice in the Arctic further suggests that the historical minimum value of sea ice was mainly attributed to the KESS region (KESS shading in Fig. 10), where sea ice—both in autumn and in October—was at its lowest since 1979. The abnormally low KESS sea-ice conditions in autumn may have provided a key precursor to the jet dynamics that occurred later that winter. This differs from many previous studies (Luo et al., 2016, 2017) that focused only on sea ice in the Barents–Kara Seas.

At the same time, from September 2020 to January 2021, several consecutive persistent UB episodes occurred (gray flow lines in Fig. 10), especially during the cold season, which, on the one hand, significantly slowed down the seasonal intensification of the westerly jet and the polar vortex, and on the other hand created a strong tropospheric-to-stratospheric EP flux upward from the Ural region (arrows a in Fig. 10), which further weakened the polar vortex (polar vortex in Fig. 10) through seasonal cumulative effects. The prolonged NAO− that persisted from December 2020 to January 2021 also led to a weakening of the mid- and high-latitude westerly jet over the North Atlantic and western Europe (NAO− in Fig. 10). In addition, on synoptic time scales, each UB caused a significant SAT decline (cold events) in China and a notable loss of sea ice in the KESS region (red and blue shading in Fig. 10). The physical mechanisms underlying the effects of the UB on sea ice and SAT have received much attention among researchers (Luo et al., 2016, 2017; Tyrlis et al., 2019). Here, we have further demonstrated the seasonal cumulative and combined effect of several UB processes across seasons. The seasonal cumulative impact of several UB episodes from early to late December 2020 led to several consecutive cooling processes in China

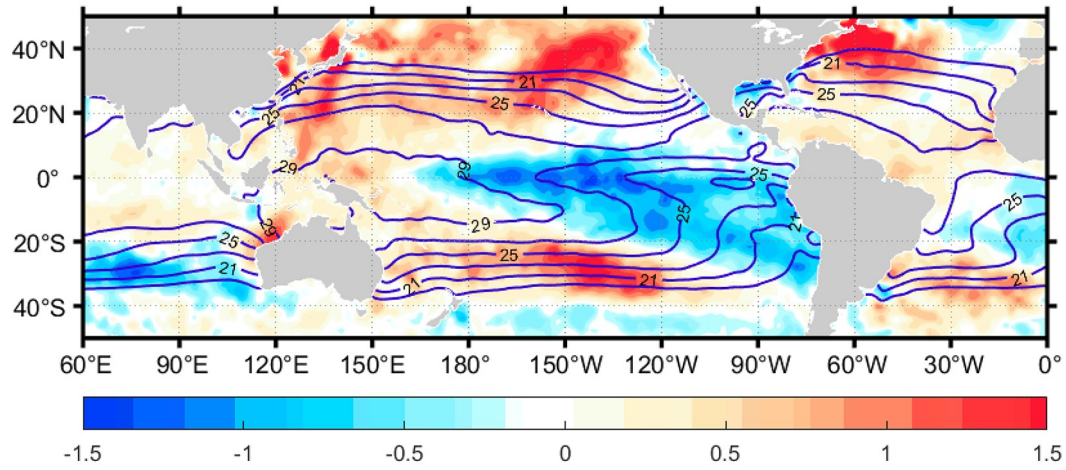

Fig. 9. Spatial distributions of December SST (units: K) for the 1979–2020 mean climatology (contours) and anomaly pattern in 2020 (shading).

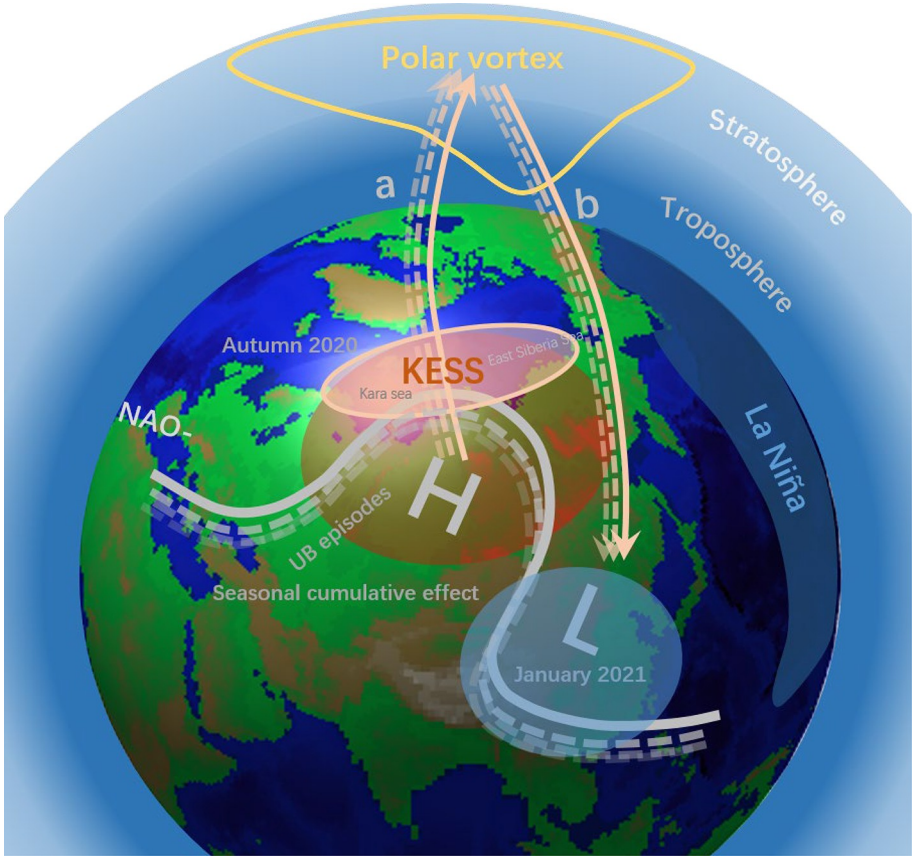

Fig. 10. Schematic diagram of the physical processes leading to the cold events in early winter 2020/21. The thick gray solid line over the Eurasian continent represents the flow line of the UB. The letter H (L) represents the anticyclonic (cyclonic) center of the UB. Red (blue) shading indicates the warming (cooling) caused by UB. KESS marks the Kara and East Siberia Seas with abnormal sea-ice cover. The upward-pointing arrows (a) indicate the propagation of EP fluxes from the troposphere to the stratosphere (weakening of the polar vortex) associated with several UB episodes. The downward-pointing arrows (b) highlight the break-up of the polar vortex and its associated several cold air outbreaks in East Asia. The light blue shading in the central-eastern Pacific represents the cold SST anomaly due to La Niña. NAO– indicates the negative NAO phase starting from December 2020. The dashed lines represent the several UBs and associated processes that occur across seasons (from Sep 2020 to Jan 2021), which is referred to as the seasonal cumulative effect.

as indicated in Fig. 6b. Several episodes of upward EP flux (Fig. 8a) and sea ice decline (Fig. 6b) due to several consecutive UBs (Fig. 6, gray vertical stripes) exert a seasonal cumulative impact upon the occurrence of several extreme cold episodes (Fig. 6b, black boxes). In the schematic diagram (Fig. 10), we use the dashed lines to represent the several UBs and associated processes that occur across seasons from September 2020 to January 2021), which is referred to as the seasonal cumulative effect in this study. In fact, several UBs also caused three significant cooling episodes between December and early January (Fig. 6b), although their specific physical processes would have differed. In addition, the three UBs and their corresponding processes provided a favorable meridional anomalous circulation (weak westerly jet) for the record-breaking extreme cold event outbreak in early January, through a seasonal cumulative effect.

It is worth noting that there was also a long-lasting UB episode in early September and one in early October. Significant KESS sea-ice decline was observed during these two UB episodes (Fig. 6b). In general, the Arctic sea ice reaches its minimum coverage by mid-September. Here, the seasonal reduction in KESS sea ice from 1 September to 16 September included an additional reduction due to warming caused by the UB. This reduction, combined with the persistent UB episode in late September/early October, weakened the rapid seasonal increase in sea ice that would have been normally been expected in October. This was likely one of the important factors contributing to the historical sea-ice minimum in the KESS region in October (autumn), at least from an atmospheric circulation perspective.

Finally, the combination of abnormally cold SSTs in the central-eastern Pacific (a La Niña year), starting in August, and an abnormal KESS warming, starting in autumn, led to a further weakening of the meridional temper-

ature gradient across the Eurasian region. This unstable temperature structure and weakened westerly jet provided for a favorable climatic background for the establishment and intensification of an anomalous meridional circulation (i.e., UB) in later winter. Although the winter SATs in China were warmer in 2020/21 compared to climatology because of the extreme warm condition observed during the later winter (not shown), the frequency and amplitude of SAT fluctuations (decline) during pre-winter (Dec 2020 to Jan 2021) have become greater due to several UB episodes and associated processes. However, the numerous cold events of the pre-winter and the warm anomalies experienced later that winter were not contradictory. This is likely related to the shift of the AO (NAO) from a predominantly negative phase to a positive phase in late February (February), with the positive phase AO characterized by a stable polar vortex structure that is also not conducive to the appearance of rapid disturbances. It is also highly likely that some other, stronger atmospheric or oceanic signal (e.g., the winter monsoon) intervened to influence the continuation of the cumulative seasonal effect, which needs to be further explored in the future.

In fact, each extreme cold spell has certain commonalities, but there are also unusual aspects. These unusual aspects are similar to the nonlinear problem in atmospheric dynamics, which has a high degree of uncertainty and chaos. Nonetheless, this study provides a reference for understanding the physical mechanisms of such extreme cold weather. Also, the pre-existing anomalous climate signal in early autumn can be regarded as a potential predictor to be used in forecasting. In addition, the issue concerning the sea-ice cover minimum in autumn 2020 will need to be further examined in future work.

Acknowledgements. The authors acknowledge the financial support from the National Natural Science Foundation of China (Grants Nos. 41975068, 41790473, and 41975099) and the Chinese Academy of Sciences Strategic Priority Research Program (Grant No. XDA19070403).

REFERENCES

Andrews, D. G., and M. E. McIntyre, 1978: Generalized Eliassen-Palm and Charney-Drazin theorems for waves on axismmetric mean flows in compressible atmospheres. *J. Atmos. Sci.*, **35**, 175–185, https://doi.org/10.1175/1520-0469(1978)035<0175:GEPACD>2.0.CO;2.

Benedict, J. J., S. Lee, and S. B. Feldstein, 2004: Synoptic view of the North Atlantic oscillation. *J. Atmos. Sci.*, **61**, 121–144, https://doi.org/10.1175/1520-0469(2004)061<0121:SVOTNA>2.0.CO;2.

Chen, X. D., D. H. Luo, S. B. Feldstein, and S. Lee, 2018: Impact of winter Ural blocking on Arctic Sea Ice: Short-time variability. *J. Climate*, **31**, 2267–2282, https://doi.org/10.1175/JCLI-D-17-0194.1.

Cohen, J., K. Pfeiffer, and J. A. Francis, 2018a: Warm Arctic episodes linked with increased frequency of extreme winter weather in the United States. *Nature Communication*, **9**, 869, https://doi.org/10.1038/s41467-018-02992-9.

Cohen, J., and Coauthors, 2014: Recent Arctic amplification and extreme mid-latitude weather. *Nature Geoscience*, **7**, 627–637, https://doi.org/10.1038/ngeo2234.

Cohen, J., and Coauthors, 2018b: Arctic change and possible influence on mid-latitude climate and weather. *US CLIVAR Report*, 41pp.

Dai, A. G., and M. R. Song, 2020: Little influence of Arctic amplification on mid-latitude climate. *Nature Climate Change*, **10**, 231–237, https://doi.org/10.1038/s41558-020-0694-3.

Ding, S. Y., B. Y. Wu, and W. Chen, 2021: Dominant characteristics of early autumn Arctic Sea Ice variability and its impact on Winter Eurasian Climate. *J. Climate*, **34**, 1825–1846, https://doi.org/10.1175/JCLI-D-19-0834.1.

Ding, Y. H., Z. Y. Wang, Y. F. Song, and J. Zhang, 2008: The unprecedented freezing disaster in January 2008 in Southern China and its possible association with the global warming. *Acta Meteorologica Sinica*, **22**, 538–558.

Edmon, H. J. J., B. J. Hoskins, and M. E. Mcintyre, 1980: Eliassen-Palm cross sections for the troposphere. *J. Atmos. Sci.*, **37**, 2600–2616, https://doi.org/10.1175/1520-0469(1980)037<2600:EPCSFT>2.0.CO;2.

Francis, J. A., S. J. Vavrus, and J. Cohen, 2017: Amplified Arctic warming and mid-latitude weather: New perspectives on emerging connections. *Wiley Interdisciplinary Reviews: Climate Change*, **8**, e474, https://doi.org/10.1002/WCC.474.

Gao, Y. Q., and Coauthors, 2015: Arctic Sea Ice and Eurasian climate: A review. *Adv. Atmos. Sci.*, **32**, 92–114, https://doi.org/10.1007/s00376-014-0009-6.

Gong, T. T., and D. H. Luo, 2017: Ural blocking as an amplifier of the Arctic Sea Ice decline in winter. *J. Climate*, **30**, 2639–2654, https://doi.org/10.1175/JCLI-D-16-0548.1.

Han, Z., and S. L. Li, 2018: Precursor role of winter sea-ice in the Labrador Sea for following-spring precipitation over southeastern North America and western Europe. *Adv. Atmos. Sci.*, **35**, 65–74, https://doi.org/10.1007/s00376-017-6291-3.

Herring, S. C., A. Hoell, M. P. Hoerling, J. P. Kossin, C. J. Schreck III, and P. A. Stott, 2016: Introduction to explaining extreme events of 2015 from a climate perspective. *Bull. Amer. Meteor. Soc.*, **97**, S1–S3, https://doi.org/10.1175/BAMS-D-16-0313.1.

Hersbach, H., and D. Dee, 2016: ERA5 reanalysis is in production. ECMWF Newsletter, No. 147, ECMWF, Reading, United Kingdom. Available from https://www.ecmwf.int/en/newsletter/147/news/era5-reanalysis-production.

Hui, G., 2009: China's snow disaster in 2008, who is the principal player. . *International Journal of Climatology*, **29**,

2191–2196, https://doi.org/10.1002/joc.1859.

Iwasaki, T., T. Shoji, Y. Kanno, M. Sawada, M. Ujiie, and K. Takaya, 2014: Isentropic analysis of polar cold airmass streams in the Northern Hemispheric winter. *J. Atmos. Sci.*, **71**, 2230–2243, https://doi.org/10.1175/JAS-D-13-058.1.

Kodera, K., H. Mukougawa, and A. Fujii, 2013: Influence of the vertical and zonal propagation of stratospheric planetary waves on tropospheric blockings. *J. Geophys. Res.: Atmos.*, **118**, 8333–8345, https://doi.org/10.1002/jgrd.50650.

Li, F., and H. J. Wang, 2012: Autumn sea ice cover, winter Northern Hemisphere annular mode, and winter precipitation in Eurasia. *J. Climate*, **26**, 3968–3981, https://doi.org/10.1175/JCLI-D-12-00380.1.

Li, H. X., H. P. Chen, H. J. Wang, J. Q. Sun, and J. H. Ma, 2018: Can Barents Sea ice decline in spring enhance summer hot drought events over northeastern China. . *J. Climate*, **31**, 4705–4725, https://doi.org/10.1175/JCLI-D-17-0429.1.

Li, M. Y., Y. Yao, I. Simmonds, D. H. Luo, L. H. Zhong, and X. D. Chen, 2020: Collaborative impact of the NAO and atmospheric blocking on European heatwaves, with a focus on the hot summer of 2018. *Environmental Research Letters*, **15**, 114003, https://doi.org/10.1088/1748-9326/aba6ad.

Lü, Z. Z., S. P. He, F. Li, and H. J. Wang, 2019: Impacts of the autumn Arctic Sea Ice on the intraseasonal reversal of the winter Siberian high. *Adv. Atmos. Sci.*, **36**, 173–188, https://doi.org/10.1007/s00376-017-8089-8.

Lü, Z. Z., F. Li, Y. J. Orsolini, Y. Q. Gao, and S. P. He, 2020: Understanding of European cold extremes, sudden stratospheric warming, and Siberian snow accumulation in the winter of 2017/18. *J. Climate*, **33**, 527–545, https://doi.org/10.1175/JCLI-D-18-0861.1.

Luo, B. H., D. H. Luo, L. X. Wu, L. H. Zhong, and I. Simmonds, 2017: Atmospheric circulation patterns which promote winter Arctic sea ice decline. *Environmental Research Letters*, **12**, 054017, https://doi.org/10.1088/1748-9326/AA69D0.

Luo, D. H., 2005: A barotropic envelope Rossby soliton model for block-eddy interaction. *Part I: Effect of topography. J. Atmos. Sci.*, **62**, 5–21, https://doi.org/10.1175/1186.1.

Luo, D. H., and J. Cha, 2012: The North Atlantic oscillation and the North Atlantic jet variability: Precursors to NAO regimes and transitions. *J. Atmos. Sci.*, **69**, 3763–3787, https://doi.org/10.1175/JAS-D-12-098.1.

Luo, D. H., Y. Yao, and S. B. Feldstein, 2014: Regime transition of the North Atlantic oscillation and the extreme cold event over Europe in January-February 2012. *Mon. Wea. Rev.*, **142**, 4735–4757, https://doi.org/10.1175/MWR-D-13-00234.1.

Luo, D. H., Y. Yao, A. G. Dai, and S. B. Feldstein, 2015: The positive North Atlantic oscillation with downstream blocking and middle east snowstorms: The large-scale environment. *J. Climate*, **28**, 6398–6418, https://doi.org/10.1175/JCLI-D-15-0184.1.

Luo, D. H., Y. Q. Xiao, Y. Yao, A. G. Dai, I. Simmonds, and C. L. E. Franzke, 2016: Impact of Ural blocking on winter warm Arctic-cold Eurasian anomalies. *Part I: Blocking-induced amplification. J. Climate*, **29**, 3925–3947, https://doi.org/10.1175/JCLI-D-15-0611.1.

Ma, S. M., and C. W. Zhu, 2019: Extreme Cold Wave over East Asia in January 2016: A possible response to the larger internal atmospheric variability induced by Arctic warming. *J. Climate*, **32**, 1203–1216, https://doi.org/10.1175/JCLI-D-18-0234.1.

Martineau, P., G. Chen, and D. A. Burrows, 2017: Wave events: Climatology, trends, and relationship to Northern Hemisphere winter blocking and weather extremes. *J. Climate*, **30**, 5675–5697, https://doi.org/10.1175/JCLI-D-16-0692.1.

Overland, J. E., and Coauthors, 2016: Nonlinear response of mid-latitude weather to the changing Arctic. *Nature Climate Change*, **6**, 992–999, https://doi.org/10.1038/NCLIMATE3121.

Shen, X. C., L. Wang, and S. Osprey, 2020: The Southern Hemisphere sudden stratospheric warming of September 2019. *Science Bulletin*, **65**(21), 1800–1802, https://doi.org/10.1016/j.scib.2020.06.028.

Tibaldi, S., and F. Molteni, 1990: On the operational predictability of blocking. *Tellus A*, **42**, 343–365, https://doi.org/10.3402/TELLUSA.V42I3.11882.

Tyrlis, E., E. Manzini, J. Bader, J. Ukita, H. Nakamura, and D. Matei, 2019: Ural blocking driving extreme Arctic Sea Ice loss, cold eurasia, and stratospheric vortex weakening in autumn and early winter 2016–2017. *J. Geophys. Res.: Atmos.*, **124**, 11313–11329, https://doi.org/10.1029/2019JD031085.

Whan, K., F. Zwiers, and J. Sillmann, 2016: The influence of atmospheric blocking on extreme winter minimum temperatures in North America. *J. Climate*, **29**, 4361–4381, https://doi.org/10.1175/JCLI-D-15-0493.1.

Wu, B. Y., 2017: Winter atmospheric circulation anomaly associated with recent Arctic Winter warm anomalies. *J. Climate*, **30**, 8469–8479, https://doi.org/10.1175/JCLI-D-17-0175.1.

Wu, B. Y., J. Z. Su, and R. D'Arrigo, 2015: Patterns of Asian winter climate variability and links to Arctic Sea Ice. *J. Climate*, **28**, 6841–6858, https://doi.org/10.1175/JCLI-D-14-00274.1.

Wu, B. Y., K. Yang, and J. A. Francis, 2017: A cold event in Asia during January-February 2012 and its possible association with Arctic Sea Ice loss. *J. Climate*, **30**, 7971–7990, https://doi.org/10.1175/JCLI-D-16-0115.1.

Wu, Z. W., J. P. Li, Z. H. Jiang, and J. H. He, 2011: Predictable climate dynamics of abnormal East Asian winter monsoon: Once-in-a-century snowstorms in 2007/2008 winter. *Climate Dyn.*, **37**, 1661–1669, https://doi.org/10.1007/s00382-010-0938-4.

Yamaguchi, J., Y. Kanno, G. X. Chen, and T. Iwasaki, 2019: Cold air mass analysis of the record-breaking cold surge event over East Asia in January 2016. *J. Meteor. Soc. Japan. Ser. II*, **97**, 275–293, https://doi.org/10.2151/jmsj.2019-015.

Yao, Y., and D. H. Luo, 2014: Relationship between zonal position of the North Atlantic oscillation and Euro-Atlantic blocking events and its possible effect on the weather over Europe. *Science China Earth Sciences*, **57**, 2628–2636, https://doi.org/10.1007/s11430-014-4949-6.

Yao, Y., and D. H. Luo, 2018: An asymmetric spatiotemporal connection between the Euro-Atlantic blocking within the NAO life cycle and European climates. *Adv. Atmos. Sci.*, **35**, 796–812, https://doi.org/10.1007/s00376-017-7128-9.

Yao, Y., D. H. Luo, A. G. Dai, and S. B. Feldstein, 2016: The positive North Atlantic oscillation with downstream blocking and middle east snowstorms: Impacts of the North Atlantic jet. *J. Climate*, **29**, 1853–1876, https://doi.org/10.1175/JCLI-D-15-0350.1.

Yao, Y., D. H. Luo, A. G. Dai, and I. Simmonds, 2017: Increased Quasi stationarity and persistence of winter Ural blocking

and Eurasian extreme cold events in response to Arctic warming. *Part I: Insights from observational analyses. J. Climate*, **30**, 3549–3568, https://doi.org/10.1175/JCLI-D-16-0261.1.

Zhang, R. N., C. H. Sun, R. H. Zhang, W. J. Li, and J. Q. Zuo, 2019: Role of Eurasian snow cover in linking winter-spring Eurasian coldness to the autumn Arctic Sea Ice retreat. *J. Geophys. Res.: Atmos.*, **124**, 9205–9221, https://doi.org/10.1029/2019JD030339.

Zheng, F., and Coauthors, 2021: The 2020/21 extremely cold winter in China influenced by the synergistic effect of La Niña and warm Arctic. *Adv. Atmos. Sci.*, https://doi.org/10.1007/s00376-021-1033-y. (in press)